Nanoscale

PAPER

View Article Online
View Journal | View Issue

Cite this: *Nanoscale*, 2023, **15**, 18265

Anticancer and antibacterial properties of carbon nanotubes are governed by their functional groups†

Aleksandra Benko, *[a,b] David Medina-Cruz, [b] Sebastian Wilk, [a] Magdalena Ziąbka, [a] Barbara Zagrajczuk, [a,c] Elżbieta Menaszek, [c] Olga Barczyk-Woźnicka, [d] Grégory Guisbiers [e] and Thomas J. Webster [f,g,h]

Due to their high strength, low weight, and biologically-inspired dimensions, carbon nanotubes have found wide interest across all of medicine. In this study, four types of highly dispersible multi-walled carbon nanotubes (CNTs) of similar dimensions, but slightly different chemical compositions, were compared with an unmodified material to verify the impact their surface chemistry has on cytocompatibility, anticancer, inflammation, and antibacterial properties. Minute changes in the chemical composition were found to greatly affect the biological performance of the CNTs. Specifically, the CNTs with a large number of carbon atoms with a +2 coordination number induced cytotoxicity in macrophages and melanoma cells, and had a moderate antibacterial effect against Gram-positive (*S. aureus*) and Gram-negative (*E. coli*) bacteria strains, all while being cytocompatible towards human dermal fibroblasts. Moreover, substituting some of the OH groups with ammonia diminished their cytotoxicity towards macrophages while still maintaining the aforementioned positive qualities. At the same time, CNTs with a large number of carbon atoms with a +3 coordination number had a high innate cytocompatibility towards normal healthy cells but were toxic towards cancer cells and bacteria. The latter was further boosted by reacting the CNTs' carboxyl groups with ammonia. Although requiring further analyses, the results of this study, thus, introduce new CNTs that without drugs can treat cancer, inflammation, and/or infection while still remaining cytocompatible with mammalian cells.

Received 19th June 2023,
Accepted 2nd October 2023

DOI: 10.1039/d3nr02923a

rsc.li/nanoscale

1. Introduction

Carbon nanomaterials, particularly carbon nanotubes (CNTs), have emerged as attractive candidates for the selective delivery of drugs, antibiotics, and other bioactive compounds inside living cells, including bacteria, cancer cells, immune cells, and/or healthy cells.[1,2] Their attractiveness lies in the fact that they can enter cells through different pathways: *via* passive diffusion or dynamin-dependent uptake.[3–5] Apart from releasing specific cargo, CNTs can also: affect cellular activity, visualize specific cells, or damage them through photothermal or photodynamic effects.[1,2,6,7] Importantly, through specific chemical modification, the CNTs internalization can be selective, targeting only a desired cell type. As such, they are often suggested as one of the possible ways to overcome the ever-growing healthcare threat of drug resistant bacteria, immune cells, and cancer cells.[8–10]

CNTs uptake and their mechanism of internalization depend on their dispersibility in polar liquids (such as those in bodily fluids, water, culture media, *etc.*), their dimensions (including aspect ratio), and surface chemistry.[4] The same properties also determine their cytoxicity to healthy cells. It is now becoming apparent that short, 15–40 nm thick, highly functionalized, and easily dispersible CNTs are cytocompatible to mammalian cells[3,11] and may also be enzymatically biodegradable, providing significant promise for numerous

[a]*AGH University of Krakow, Faculty of Materials Science and Ceramics, A. Mickiewicz 30 Ave., 30-059 Krakow, Poland. E-mail: abenko@agh.edu.pl; Tel: +48 12 617 52 06*
[b]*Department of Chemical Engineering, Northeastern University, 360 Huntington Ave., Boston, MA, USA*
[c]*Department of Cytobiology, Collegium Medicum, Jagiellonian University, 9 Medyczna St., 30-068 Krakow, Poland*
[d]*Department of Cell Biology and Imaging, Jagiellonian University, 9 Gronostajowa St, 30-387, Kraków, Poland*
[e]*Department of Physics and Astronomy, University of Arkansas at Little Rock, 2801 South University Avenue, Little Rock, AR 72204, USA*
[f]*Department of Biomedical Engineering, Hebei University of Technology, Tianjin, China*
[g]*School of Engineering, Saveetha University, Chennai, India*
[h]*UFPI - Universidade Federal do Piauí, Brazil*

†Electronic supplementary information (ESI) available: Additional SEM and TEM images of the samples, different visualizations of the cytotoxicity, proliferation, and viability results. See DOI: https://doi.org/10.1039/d3nr02923a

medical applications.[12,13] Herein, surface chemistry is also the key to the selectivity of CNTs to cells, by which they can be benign to normal and healthy cells but detrimental to cancer cells or pathogens, such as bacteria and even viruses.[1]

In our previous studies, we found that cytocompatible medical device surfaces can be fabricated by depositing CNT layers onto the surface of titanium.[14–16] Recently, anti-cancer and anti-bacterial properties were reported, which correlated with the surface chemistry affecting CNTs' electro-donor properties and reactive oxygen species (ROS) activity.[17] The same differently functionalized CNTs embedded inside the carbon nanofibers (which could be regarded as highly defected, non-hollow versions of CNTs) also caused significant changes to their antibacterial properties.[18] Specifically, when deposited as layers or embedded inside the carbon nanofibers, CNTs with carbon at a +3 oxidation number (and their amidized derivatives) demonstrated the greatest cytocompatibility properties of all of the materials investigated, combined with the best antibacterial performance.

This study was designed to verify how different surface chemistry modifications can affect the functional performance of the CNTs administered to cells in free form (*i.e.*, as it would be for their application in drug delivery purposes). In this study, four CNTs types, differing in their surface chemistry, were employed. These were: HO (highly oxidized CNTs with a high share of –C═O bonds), LO (low oxidized CNTs with a high share of –C–O bonds), and two types of ammonia-modified CNTs derived from the oxidized ones: HNH and LNH, respectively. CNTs differed in their surface chemistry but were of similar sizes. Unmodified and longer CNTs served as a control. The full physicochemical characteristics of the CNTs used here can be found in our previous study,[19] and these are also listed in Table 1. The optimal goal was to obtain CNTs, which on the one hand, are relatively benign to healthy cells, but on the other hand, can target cancer cells, immune cells, and bacteria. Within this study, possible uptake mechanisms that change depending on CNT surface chemistry were also analyzed. Human dermal fibroblasts and macrophages were selected as healthy cells, the first serving as model cells, the second being the body's first line of defense against possibly unwanted particles and/or pathogens. Melanoma cells served as a model cancer cell line and two bacteria strains were used for the evaluation of both Gram-negative (multidrug-resistant *Escherichia coli* (MDR-EC)) and Gram-positive (Methicillin-resistant *Staphylococcus aureus* (MRSA)) bacteria.

2. Materials and methods

2.1. Functionalized CNTs

The as-received, unmodified MWCNTs (NanoAmor, USA, stock #1213NMGS,[20] referred to as uCNTs throughout this study) were subjected to chemical oxidation in mixtures of sulfuric (H_2SO_4) and nitric (HNO_3) acids, as described in our previous study.[14,19] Briefly, highly oxidized CNTs (HO) were obtained by using a 3 : 1 sulfuric to nitric acid ratio, while the low oxidized (LO) used a 1.5 : 1 ratio. Each CNT type was heated in the acids (1 : 100 by wt) for a total of 22 h, and the acidic residues and the reaction by-products were washed off during centrifugation. This was conducted until a neutral pH of the supernatant was reached. The as-obtained CNTs were dried and stored for further use. Subsequently, the oxygen-based functional groups (carboxy and hydroxy) were dehydrogenated by dicyclohexylcarbodiimide (DCC) and reacted with ammonia to form amide/amine functional groups. Thus, HNH (highly oxidized and ammonia-modified CNTs) and LNH (low oxidized and ammonia-modified CNTs) were obtained. Full experimental details of the MWCNT fabrication process can be found as published in our recent study.[19] In the cited study, a thorough investigation of the CNTs physicochemical properties can be found, and a summary of these properties is given in Table 1.

Table 1 Summary of the physicochemical properties of CNTs used in this study. Based on the analysis presented in ref. 19

	uCNTs	HO	LO	HNH	LNH
Oxygen content[a]	<2%	16.0%	14.9%	12.1%	11.9%
C/O[a]	n/a	5.3	5.7	7.1	7.2
Nitrogen content[a]	0%	0%	0%	2.3%	2.0%
N_R	N	0	0	0.16	0.14
O_R	N	1	1	0.84	0.86
C–X[b] bonds[a]	n/a	19.5%	29.5%	15.8%	18.5%
C═O bonds[a]	n/a	29%	18.1%	20.5%	16.7%
Length range [nm][c]	10 000–30 000	100–800	100–1200	100–800	100–1200
Diameter [nm][c]	10–50				
Work function	4.60 ± 0.01 eV	4.84 ± 0.01 eV	4.94 ± 0.01 eV	4.57 ± 0.01 eV	4.35 ± 0.01 eV
Dipole moment normal to the surface (most distinctive functional group)	n/a	−0.02 a.u. (COOH)	−0.61 a.u. (COH)	0.21 a.u. (CONH)	0.07 a.u. (CNH_2)
Overall surface charge	Neutral	Negative	Negative	Negative	Negative
Average current flow during electrophoretic deposition at 30 V	n/a	1.2 mA	0.8 mA	2 mA	1.8 mA
Tendency to agglomerate	High	Low	Moderate	Low	Moderate

[a] As identified by XPS; N_R is the share of nitrogen atoms related to a total amount of oxygen (O_R). [b] X is carbon, oxygen, or nitrogen. [c] As identified by analyzing the TEM data through the ImageJ software.

2.2. CNT structure and degree of chemical modification

The structural changes and the number of functional groups introduced through the above-mentioned wet chemistry methods were already analyzed in our previous study, using X-ray photoelectron spectroscopy (XPS), Fourier-transform infrared spectroscopy (FTIR), and Raman spectroscopy. Transmission electron microscopy (TEM) was used to evaluate the lengths and visualize possible changes in the structure. Two samples were additionally subjected to the thermogravimetric analysis (TGA), with results found in the ESI.†[19] This data is summarized in Table 1. Briefly, the employed chemical oxidation shortens the CNTs and introduces up to 16 at% of oxygen. In HO, higher amounts of polar carboxyl groups led to a reduced agglomeration and sedimentation tendency. Meanwhile, hydrophobic uCNTs that are prone to form π–π interactions along their sidewalls, are poorly dispersible and sediment spontaneously in polar fluids. Smaller and less polar groups abundant in LO and LNH (OH and NH_2, respectively) also do not provide sufficient repulsive forces to overcome the π–π attractions and thus, these CNTs are prone to partial agglomeration and sedimentation (still, to a much smaller extent than found in uCNTs). The susceptibility of the CNTs studied to form agglomerates were further visualized through low-magnification TEM observations (ESI 1†).

In this study, we performed an additional thermal analysis to confirm the amount and type of surface functional groups on all the CNTs. We believe that such an extensive analysis of the CNTs is necessary to fully understand the mechanism by which bacteria and cells respond to the materials. TGA was performed using an STA 449 F3 Jupiter, Netzsch device. Approximately 5 mg of each CNT type was separately placed inside a standard alumina crucible. Nitrogen flow at a 50 ml min^{-1} rate was used as a protective atmosphere to avoid combustion. The samples were then heated from 40 to 1200 °C at a rate of 20 °C min^{-1}. At least three separate measurements were conducted on each sample type, and the data presented are the mean values from all of the measurements. The TG curves were analyzed using Proteus 6.1 software, while the calculations and data presentation were completed in Excel 365 and Origin 2021 software. The presented averaged plots were smoothed in Origin 2021 (Savitzky–Golay method, with 100 points of window and polynomial order of 2). To identify changes in the mass loss rate, indicative of a chemical reaction (or decomposition of certain functional groups), the 1st derivative (DTG) of each curve was calculated.

Typically, TG curves are represented as the percentage of the mass loss related to initial mass (assumed to be 100%). Because functional groups in the CNTs are related to the presence of atoms with different atomic masses, for better comparison with the XPS data, our results were normalized to the atomic mass of carbon, oxygen, and nitrogen, using Formulae (1). By this means, the total amount of residual carbon (TA_C), released oxygen (TA_O) and released nitrogen (TA_N) atoms were calculated for each sample, at a temperature of 900 °C – above this temperature, thermal decomposition of amorphous carbon is assumed to occur, so further mass loss is not solely due to the presence of heteroatoms.[21] Additionally, mass loss steps, expressed as the percentage of mass lost at certain temperature ranges, can be attributed to the decomposition of functional groups, which were also normalized to the total mass of oxygen and nitrogen atoms in the samples ($TA_N + TA_O$).

Equations are used to normalize the mass lost during the thermal decomposition of the samples by the atomic mass of the atoms present in the sample. M_{900} is residual mass at 900 °C, O_R is a share of oxygen atoms related to the total amount of oxygen and nitrogen atoms, N_R is a share of nitrogen atoms related to the total amount of oxygen and oxygen atoms. O_R and N_R are calculated from the XPS results and given in Table 2.

$$TA_C = \frac{M_{900} \times 12}{M_{900} \times 12 + (100 - M_{900}) \times 16 \times O_R + (100 - M_{900}) \times 14 \times N_R} \times 100\%$$

$$TA_O = \frac{(100 - M_{900}) \times 16 \times O_R}{M_{900} \times 12 + (100 - M_{900}) \times 16 \times O_R + (100 - M_{900}) \times 14 \times N_R} \times 100\%$$

$$TA_N = TA_C - TA_O \quad (1)$$

Table 2 Residual masses of the CNTs, left after heating the samples in an inert atmosphere and to a certain temperature, combined with the as-calculated values of the atomic compositions and functional groups

		uCNTs	HO	LO	HNH	LNH
Residual mass at 1200 °C [%]		**96.5 ± 1.1**	**83.7 ± 0.7**	**87.9 ± 2.3**	**81.0 ± 2.5**	**84.4 ± 0.0**
Residual mass at 900 °C [%]		98.2 ± 0.6	85.5 ± 1.0	89.5 ± 2.3	86.3 ± 1.2	87.4 ± 0.4
Mass lost between 900 °C and 1000 °C [%]		0.4 ± 0.2	0.6 ± 0.1	0.5 ± 0.1	1.4 ± 0.6	0.7 ± 0.2
The total amount of carbon atoms at 900 °C (TA_C) [%]		97.6 ± 0.8	81.2 ± 1.2	86.2 ± 2.8	81.6 ± 1.7	83.4 ± 0.5
The total amount of oxygen atoms at 900 °C (TA_O) [%]		2.4 ± 0.8	18.8 ± 1.2	13.7 ± 2.8	15.5 ± 1.5	9.5 ± 6.7
The total amount of nitrogen atoms at 900 °C (TA_N) [%]		0	0	0	2.9 ± 0.3	1.6 ± 1.1
Irrelative content [%]	40–150 °C hydrogen, physisorbed water[28]	0.1 ± 0.1	1.3 ± 0.9	1.1 ± 0.9	1.0 ± 0.9	0.9 ± 0.0
	150–253 °C carboxyl,[28] DCU[27]	0.1 ± 0.1	3.5 ± 0.2	2.4 ± 0.6	3.7 ± 0.3	3.9 ± 0.1
	253–315 °C lactone at zig-zag edges,[22,23] DCU residues	0.1 ± 0	1.8 ± 0.0	1.4 ± 0.2	1.7 ± 0.4	2.6 ± 0.1
	315–510 °C anhydrides, esters,[22,23] C–N bonds[29]	0.4 ± 0.2	5.3 ± 0.1	3.7 ± 0.6	7.3 ± 1.3	6.0 ± 0.5
	510–620 °C lactone at armchair edges[22,23]	0.9 ± 0.4	3.2 ± 0.2	2.3 ± 0.5	2.4 ± 0.1	2.1 ± 0.1
	620–800 °C phenol, ether, stable derivative of anhydrides[23]	0.3 ± 0.4	2.9 ± 0.4	2.2 ± 0.4	1.4 ± 0.4	0.3 ± 0.1
	800–900 °C carbonyl[23,24]	0.6 ± 0.1	0.9 ± 0.0	0.8 ± 0.0	0.9 ± 0.0	0.8 ± 0.2

2.3. Biological investigation of the CNTs

The biological studies were conducted using a series of CNT concentrations (from 0 for the control, through 25, 50, 75, and 100 μg mL^{-1}) to test the impact of increasing nanomaterials concentration on the number of normal healthy cells, cancer cells, and bacteria. The CNTs were dispersed in a medium with a probe sonicator (Vibra-cell, type VCX 130 from Sonics & Materials, Inc., equipped with a 6 mm probe, operating at a 30% maximum amplitude, and for 2 minutes).

2.3.1. Cytotoxicity and ROS production in macrophages. RAW 264.7 murine macrophage cells (ATCC, USA) were expanded in Nunclon Delta 75 cm^2 culture flasks (Nunc, Denmark) and cultured in Dulbecco's Modified Eagle Medium without phenol red (DMEM, Lonza, USA), supplemented with 10% fetal bovine serum (FBS, Gibco, USA), under standard conditions (humidified atmosphere containing 5% CO_2 and at 37 °C). The culture medium was changed every three days. Cells were detached from culture flasks using TrypLE™ Select Enzyme (Gibco, USA). Cells were seeded into wells of 96-well culture plates (Corning, USA) at a density of 2×10^4 cells per well, fed with CNT modified culture medium, and cultured for 24 and 72 hours in standard culture conditions. All tests were conducted on cells with passage numbers 4 and 5.

A ToxiLight™ Non-Destructive Cytotoxicity BioAssay Kit coupled with ToxiLight™ 100% Lysis Control Set (both Lonza, USA) was applied to determine RAW cell proliferation and CNT cytotoxicity. The assay results (luminescence) were measured with an Omega POLARstar Microplate Reader (BMG Labtech, Germany). Proliferation was noted as the adenylate kinase level in cell lysates (corresponding to the number of living cells). At the same time, cytotoxicity was a proportion of adenylate kinase in culture supernatants (corresponding to the number of dead cells) to the adenylate kinase level in cell lysates.

ROS levels in cell cultures were detected with a 2′,7′-dichlorodihydrofluorescein diacetate (DCFH-DA) ROS indicator (Sigma-Aldrich, USA). Specifically, DCFH-DA powder was dissolved in DMSO (Sigma-Aldrich, USA), creating a stock solution. Before the experiment, a DCFH-DA stock was diluted in a HBSS buffer (Gibco, USA) at a 1 : 100 ratio, creating a working solution. Cell culture medium was exchanged for a DCFH-DA working solution, and the cells were further incubated at 37 °C for 30 min. The assay results (fluorescence) were collected using an Omega POLARstar Microplate Reader (BMG Labtech, Germany).

2.3.2. Cytotoxicity and ROS production in human dermal fibroblasts and cancer cells. Primary human dermal fibroblast cells (Lonza, CC-2509, AMP) and melanoma cells (ATCC® CRL-1619, Manassas, VA) were used for the cytotoxicity evaluation. The cells were cultured in DMEM, supplemented with 10% FBS, and 1% penicillin/streptomycin. Cells were seeded onto tissue-culture-treated 96-well plates (Thermo Fisher Scientific, Waltham, MA), at a concentration of 5000 cells per well, in 100 μL of DMEM. After a 24 h incubation (at 37 °C, in a humidified incubator with 5% CO_2), the culture medium was replaced with 100 μL of fresh cell medium containing increasing concentrations (from 25 up to 100 μg mL^{-1}) of different CNT types. To identify the average growth of cells without CNTs, and determine the background absorbance of the media, cells cultured with pure medium, and pure medium by itself were used as controls, respectively. Cells were cultured for 24 h or 72 h in the same conditions, followed by washing with PBS, and replacing the medium with 100 μL of an MTS solution (3-(4,5-dimethylthiazol-2-yl)-5-(3-carboxymethoxyphenyl)-2-(4-sulfophenyl)-2*H*-tetrazolium, CellTiter 96® Aqueous One Solution Cell Proliferation Assay, Promega, Madison, WI, mixing ratio of 1 : 5 of MTS : medium), which was used to assess the cell metabolic activity. After adding the solution, the 96-well plate was incubated for an additional 4 h to allow for a color change. Then, the absorbance was measured at 490 nm on an absorbance plate reader (SpectraMAX M3, Molecular Devices).

For ROS analysis of melanoma cells, the cells were cultured for 24 h as described above. The ROS indicator was reconstituted in DMSO to make a concentrated stock solution that was kept and sealed. The growth media was then carefully removed, and 10 μM of the indicator in PBS was added to each of the wells. The cells were incubated for 30 min at 37 °C, and the loading buffer was removed afterwards. Fresh media was added, and cells were allowed to recover quickly. The baseline was determined by measuring the fluorescence intensity of cells loaded with the ROS indicator before excitation at 485 nm. Positive controls were included by stimulating the oxidative activity with hydrogen peroxide to a final concentration of 50 μM. The intensity of fluorescence was then observed by flow cytometry. Measurements were taken at a fluorescence wavelength at 530 nm when the samples were excited at 485 nm. Fluorescence was also determined in the negative control – untreated cells loaded with the dye and maintained in a buffer.

2.3.3. Microscopic observations of cells. A Nova NanoSEM 200 scanning electron microscope (FEI, Eindhoven, The Netherlands) was used to visualize cell attachment, proliferation, and morphology after being cultured with CNT-modified medium. At the end of the 7^{th} day of cell culture with CNT concentrations of 50 and 100 μg mL^{-1}, macrophages were fixed with 2% glutaraldehyde (Sigma-Aldrich) and dehydrated with graded ethanol (ranging from 20% to 100% (v/v)). Next, the samples were air-dried, mounted on SEM stubs, coated with a 6 nm thick carbon layer (Leica EM ACE600 High Vacuum Sputter Coater), and visualized. The observations occurred in low vacuum conditions (60 Pa), using a Low Vacuum Detector (LVD), and with an accelerating voltage of 10–18 kV.

For Transmission Electron Microscopy (TEM), samples were fixed in 2.5% glutaraldehyde (10×) in a 0.1 M cacodylic buffer for 18 h at 4 °C. Next, the samples were post-fixed for 1 h in 1% osmium tetroxide, and dehydrated with graded ethanol (from 50%, 70%, 90% to 100% (2 × 10 min)), followed by propylene oxide (2 × 10 min). After infiltration, samples were embedded in a PolyBed 812 kit at 60 °C.

Ultrathin sections (Leica EM UC7 microtome) were collected on copper one-slot grids, and covered with a formvar film (1% formvar in dichloroethane). Sections were contrasted by immersing in uranyl acetate and Reynold's lead citrate for 3 minutes, followed by washing in distilled water. For imaging, a JEOL JEM 2100HT electron microscope (Jeol Ltd, Tokyo, Japan) was used at an accelerating voltage of 80 kV. Images were taken by using a 4k × 4k camera (TVIPS), equipped with EMMENU software ver. 4.0.9.87.

2.3.4. Bacterial culture preparation and antibacterial analysis. Strains of both Gram-negative (multidrug-resistant *Escherichia coli* (MDR-*E. coli*) (ATCC BAA-2471; ATCC, Manassas, VA)) and Gram-positive bacteria (Methicillin-resistant *Staphylococcus aureus* (MRSA) (ATCC 4330; ATCC, Manassas, VA)) were used in this study to determine the antibacterial activity of different CNT samples. Before inoculation, the bacterial cultures were maintained on agar plates at 4 °C. Bacteria were introduced into 6 mL of sterile Luria–Bertani (LB) (bioPLUS, bioWORLD) medium in a 15 mL Falcon centrifuge tube and incubated at 37 °C/200 rpm for 24 h. The bacterial suspension was then diluted to 10^6 colony-forming units per milliliter (CFU mL^{-1}) and stored at 4 °C until use. The bacterial culture optical density (OD) was measured at 600 nm using a spectrophotometer (SpectraMax M3, Molecular Devices, Sunnyvale, CA). Growth curves and other bacterial analyses were performed using a plate reader SpectraMax® Paradigm® Multi-Mode Detection Platform.

100 μL of different concentrations of CNTs samples in LB medium were mixed with 100 μL of bacteria in LB medium and were then added to each well of a 96-well plate (Thermo Fisher Scientific, Waltham, MA). The final volume per well was 200 μL. Once the plate was prepared, the absorbance of all samples was measured at 600 nm on an absorbance plate reader, every 2 min and for 24 h with no shaking. Negative controls containing only nanoparticles and medium were used to determine the absorbance caused by the CNTs.

Colony counting assays were also performed: bacteria were seeded in a 96-well plate and treated with different concentrations of the CNTs samples for 8 h inside an incubator at 37 °C. Then, the 96-well plate was removed from the incubator, and all the samples were diluted with PBS in a series of vials to either ×100, ×1000, or ×10000. Three drops of a 10 μl aliquot of each dilution were placed in an LB-Agar plate and incubated for 8 h inside the incubator at 37 °C. The colonies formed in each plate were counted at the end of the incubation period.

2.3.5. Statistical analysis. Statistical analyses were performed using Statistica 13 software (Tibco Software, Palo Alto, CA, USA) and applying one-way analysis of variance (one-way ANOVA) with *post-hoc* Tukey's test. The data are presented as the means ± standard deviation (SD) and represent at least three independent experiments. The statistical differences were considered significant at $p < 0.05$ and were indicated by lowercase (differences between samples on day 1 of culture) and uppercase (differences between samples on day 3 of culture) letters or asterisks (differences between day 1 and 3 of culture).

3. Results and discussion

3.1. CNT chemical modification

To confirm the chemical composition of the materials, the samples were subjected to thermogravimetric analyses. The TG curves and their first derivatives are plotted in Fig. 1A and B, respectively. The same unsmoothed curves, presented along with standard deviation values, are given in ESI 1 and ESI 2.†

Values of the residual masses at two different temperatures (900 °C and 1200 °C) and the irrelative amounts of functional groups are gathered in Table 2. For better comparison, in Table ESI 1,† the relative shares of the same functional groups are given. These were calculated based on the assumption that the mass lost up to 900 °C sums up to 100% of the functional groups present in the given CNT type. The same was assumed for calculating the total amount of carbon, oxygen, and nitrogen atoms (TA_C, TA_O, and TA_N values, respectively). While being mostly true, it is important to point out that these calculations leave out part of the mass lost due to the decomposition of carbonyl and phenol functional groups. These groups start to decompose around 800 °C and end around 1000 °C.[22–24] At the same time, the decomposition of amor-

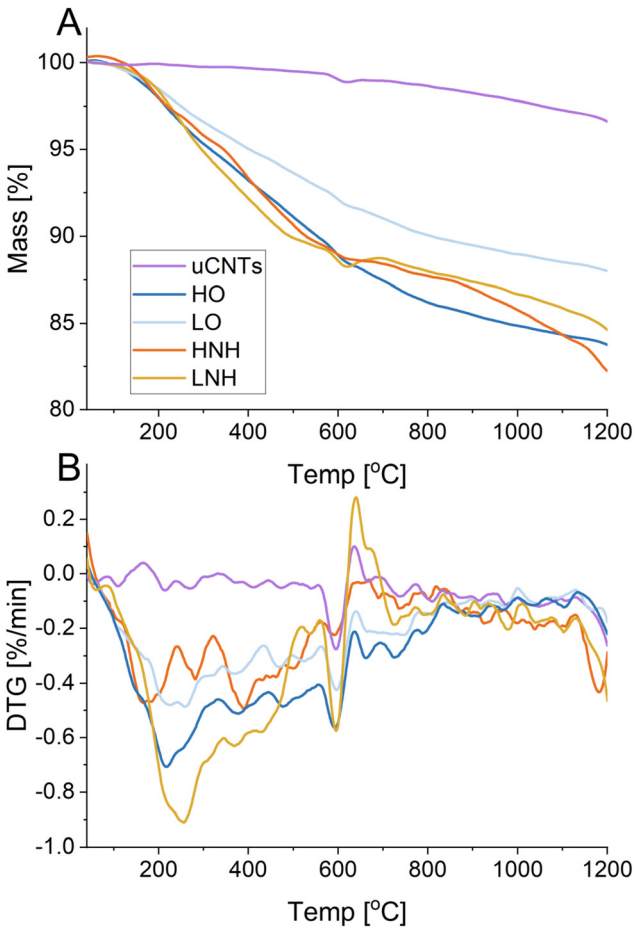

Fig. 1 Results from the TG (A) and DTG (B) analysis of the tested samples.

phous carbon has been reported to start around 900 °C.[21] Because TGA does not allow one to separate the mass lost due to two co-occurring reactions, we decided it would be best to assume that most of the functional groups were removed from the samples up to 900 °C. In most of the samples, mass lost between 900 °C and 1000 °C was between 0.4 and 0.7%, suggesting that this assumption is fairly accurate. One exception was the HNH, for which 1.4% of mass was lost in this region. HNH is derived from HO and in principle, its basic functional groups that could be stable up to 900 °C should not be significantly different from its parent structure. In our previous study, we found that some portion of nitrogen atoms in the HNH and LNH were built-in graphitic planes. These are removed above 850 °C (pyridinic) and 950 °C (quaternary).[25] At the same time, some of the nitrogen atoms may first become oxidized (above 700 °C) in the presence of residual oxygen released from the samples[26] and then decomposed above 950 °C.[25] Between the two amidized samples, HNH had higher amounts of oxygen atoms.[19] Its parent CNT (HO) also had more highly functionalized structures, likely contributing to higher reactivity and more thermally stable (up to 900 °C) nitrogen-derived functional groups. All of these factors could have resulted in increased mass reduction observed for this sample above 900 °C.

Between 40 and 150 °C, all of the tested CNTs released adsorbed water and hydrogen molecules. Similar amounts of these were reported for all of the functionalized CNTs (between 0.9–1.3%), which were higher than in the uCNTs (0.1%) (Table 2). This could be attributed to the fact that regardless of their type, polar functional groups are expected to be more favorable to water adsorption than the hydrophobic graphitic planes of uCNTs.

As reported in the literature, the next decomposition step, between 150 and 253 °C, could be attributed to the degradation of the carboxyl groups[22,23] or sublimation of dicyclohexylurea (DCU),[27] a side product of a DCC-initiated reaction. More significant mass losses were observed in the HO, HNH, and LNH samples (3.5%, 3.7%, and 3.9% respectively) than in LO (2.4%) and uCNTs (0.1%). In HNH and LNH, significant mass reduction in this region could be partially attributed to the DCU residues, which was already suggested in our previous study.[19] For the HO, which was not subjected to the DCC-activated reaction, higher mass loss in this temperature range likely indicates higher amounts of carboxyl functional groups (3.5%) than in LO (2.4%), a direct consequence of using a mixture of acids having a higher oxidation strength. These results align with the XPS analysis performed in our previous study.[19]

Advantageous over XPS, TGA allows one to differentiate between the –C–O, –C–OH, and –CHO groups, while also identifying the –C═O functional groups. Mass reduction attributed to the lactone groups (between 253 and 315 °C for zig-zag and 510–620 °C for armchair edges) was found to be the highest for the HO and HNH samples (around 5.0%), followed by LNH and LO (around 4.6%), and ending at 1% in uCNTs. HO and HNH were characterized by the highest amounts of anhydride/ester functional groups, which are released between 315 and 510 °C (5.3 and 7.3% respectively). As expected, significantly lower values of these were observed in the LO (3.7%) and uCNTs (0.1%). Surprisingly, in the LNH, a 6.2% mass reduction was observed. In both the HNH and LNH, the mass reduction in this range increased by roughly 2% as compared to their parent CNTs. Because the conducted amidizitation was performed with no additional oxidation, no new anhydride/ester functional groups could have been formed. Hence, we hypothesize that there should be some nitrogen-based derivative decomposing in this region, contributing to the increased mass loss in HNH and LNH. This could be attributed to the breaking of C–N bonds (including the ones in amide bonds) which have been reported at the onset of 300 °C.[29,30] In HNH, a well-defined peak at 393 °C is observable on the DTG curve, with a mass loss rate of −0.5 °C min^{-1}, indicative of a second decomposition happening in this sample. Meanwhile, in LNH this reaction is merely a shoulder of a fast proceeding, almost linear decomposition happening in this sample from 85 to 520 °C. Hence it can be suggested that HNH is rich in more chemical species that do not have overlapping thermal decomposition temperatures.

HO and LO had the highest shares (2.9 and 2.2%, respectively) of phenol/ether/stable derivatives of anhydride (decomposition between 620 to 800 °C). In HNH, this value was reduced to 1.4%, and LNH was characterized by the same, insignificant amount as the uCNTs (0.3%). It could be suggested that the employed amidization technique likely diminished the amount of C–O–C/COOC interactions in the parent CNTs, in favor of C–N, C═N and C═O–N. This chemical species could not be differentiated in the previously conducted XPS analysis.[19]

To sum up, the TGA analysis is a supplementary technique to the XPS evaluation, confirming major findings from XPS and allowing one to differentiate functional groups that could not have been separated by XPS. It was found that the unoxidized samples had around 2% oxygen atoms, which is in line with the technical specification provided by the producer. We found that these oxygen atoms could be in various functional groups (mainly lactone and phenol). This material is characterized by an additional 3% of amorphous carbon. Chemical oxidation removes amorphous carbon impurities while introducing oxygen-related functional groups. In an environment of higher oxidation strength (HO), carbon atoms are oxidized to higher oxidation numbers, and higher amounts of oxygen atoms are introduced.

Conversely, removing amorphous carbon is more effective in an environment with lower oxidation strengths (LO), and more oxygen atoms are introduced into the lactone positions of the armchair edges. Interestingly, TGA analysis could not differentiate between the amide/amine functional groups, as the HNH and LNH were characterized by similar mass loss kinetics. Still, it was found that in HNH, thermal degradation was initiated at lower temperatures (70 °C) but proceeded slower (peaking at 0.5% min^{-1}) than what was found in LNH (145 °C, peaking at 0.9% min^{-1}). Above 800 °C, mass loss rate

in HNH started to increase, peaking at −0.4% min^{-1} at 1180 °C. It could be hypothesized that in LNH, higher amounts of amidation reaction by-products were present, which contributed to more significant mass changes than what was expected based on their oxidation level. Meanwhile, in the HNH, higher amount of nitrogen atoms built-in graphitic planes, that were stable up to 800 °C was found. These results agree with our previous XPS analysis, where higher amounts of C=C bonds also characterized LNH, likely partially attributed to the aromatic rings of the DCU residue.[19]

3.2. Biological performance of the CNTs

3.2.1. Cytocompatibility with macrophages. Macrophages were cultured in a CNTs-supplemented culture medium (increasing concentrations of CNTs – 0, 25, 50, and 100 μg mL^{-1}) for 1 and 3 days. Afterwards, cell viability and proliferation were evaluated. Unlike other cells, macrophages will multiply when they encounter a substance they assume needs to be eliminated by phagocytosis, including unfavorable materials. Hence, an increase in the total amount of macrophages with an increasing concentration of CNTs indicates that the nanomaterials do not evade the immune response but instead stimulate macrophage division aimed at successive clearance. This doesn't necessarily mean that the materials are cytotoxic. Fig. 2 represents the total amount of cells present in the culture as a function of increasing concentrations of various CNTs. A different graphical representation of the same data can be found in ESI 4,† wherein culture times and CNT concentration are compared on the same graph, and a separate graph for each CNT type is prepared.

Analyzing the graphs in Fig. 2, it is evident that on day 1 of culture, the number of macrophages increased when the cells were cultured with 25 μg mL^{-1} of unmodified CNTs and then gradually dropped at higher concentrations. In contrast, with all of the functionalized CNTs, the number of macrophages reduced at the 25 μg mL^{-1} concentration, but to a different extent – the highest reduction (by 25%) was observed for HO, while the lowest (12%) was for HNH. The differences between the remaining CNTs are statistically insignificant at this concentration. At 50 μg mL^{-1}, the number of cells grown in contact with HNH, LNH, and HO was similar to each other and to the 25 μg mL^{-1} concentrations. Meanwhile, in the case of LO, the number of cells increased at a 50 μg mL^{-1} concentration and was similar to the value observed for uCNTs (both at 25 μg mL^{-1} and 50 μg mL^{-1}).

Further increases in the CNT concentrations caused reductions in cell numbers. At 75 μg mL^{-1}, the lowest numbers of cells were found for HNH and LNH, which were similar to the values recorded at 100 μg mL^{-1} for the rest of the samples. On day 1, there were no obvious differences between the influence of varying functional groups of CNTs and the cells appeared to be more sensitive towards increasing concentration (the cell numbers appeared to be inversely proportional to the CNT concentration).

More significant differences between CNT type and their concentration can be observed on day 3 of culture. Herein, the trend in cell number changes remained similar when increasing concentrations of uCNTs and HNH were used – for example, an increase in cell number at 25 μg mL^{-1} (comparable values between the two), followed by an almost linear reduction at 50 (comparable values) and 75 μg mL^{-1} (a lower number of cells were recorded for the HNH) were observed. At 100 μg mL^{-1}, the number of cells further dropped for the uCNTs but remained constant for the HNH (similar to day 1). The most significant reduction in the number of macrophages was observed for the LO, with similarly low values recorded

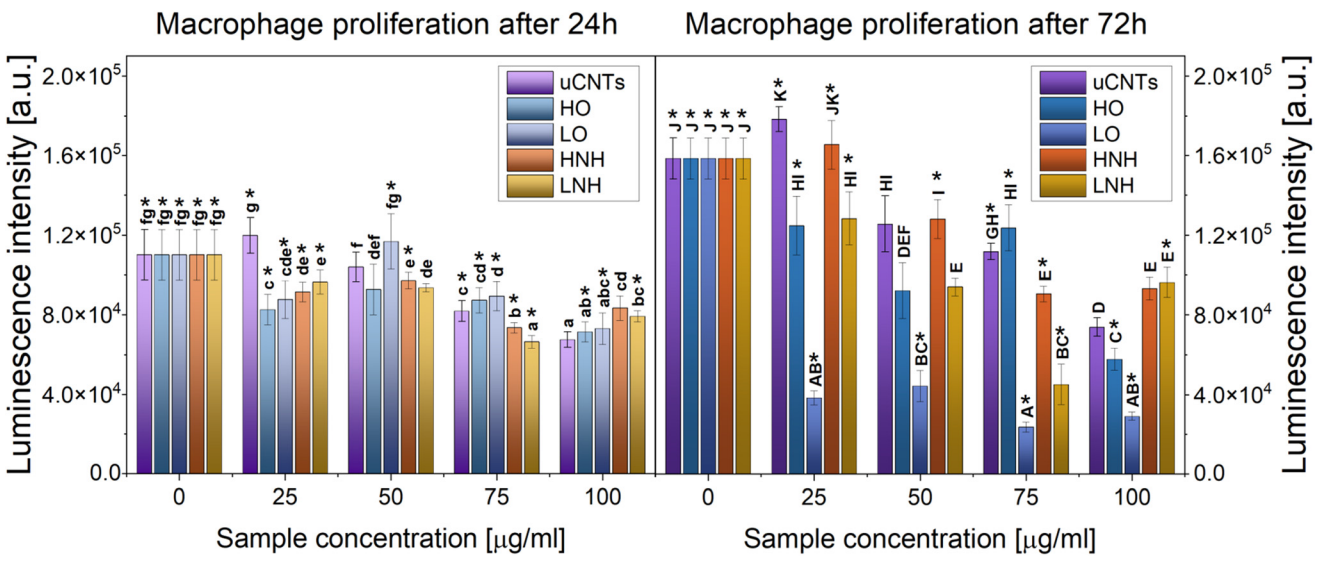

Fig. 2 Proliferation of RAW 264.7 murine macrophages cultured with CNTs, tested *via* the ToxiLight assay. The data are presented as means ± SD. Statistically significant differences ($p < 0.05$) between the tested materials compared to one another are marked a–g for the 1st day of culture and A–K for the 3rd day of culture; * indicates statistically significant differences between day 1 and day 3 of culture.

regardless of the CNT concentration. For HO, similar values were recorded at 25 and 75 μg mL^{-1}, but were slightly reduced at 50 μg mL^{-1}. This was followed by a significant reduction at 100 μg mL^{-1}. In LNH, the number of cells gradually dropped with increasing CNT concentration, then elevated at 100 μg mL^{-1}.

Low concentrations of uCNTs induced macrophage proliferation – likely, the cells were preparing for nanoparticle clearance from the system, indicating that their presence was unfavorable. A consecutive reduction in cell number at higher concentrations, and regardless of culture time, might indicate that the uCNTs are cytotoxic. On day 3 of culture, LO appeared to be the most detrimental to macrophages, independent of CNT concentration. For HO, HNH, and LNH, a progressive reduction in cell numbers with increasing concentrations was observed, with different thresholds for 50% cell number reductions. In HO, this was recorded at 100 μg mL^{-1} and 75 μg mL^{-1} could be regarded as a safe concentration. In LNH, this was observed at 75 μg mL^{-1} and 50 μg mL^{-1} could be regarded as a safe concentration. In HNH, a 50% reduction in the number of cells was never observed. Hence, the HNH appeared to be the least toxic across all CNT concentrations and culture times tested here.

To confirm the impact of CNT on cells, cytotoxicity was analyzed by calculating the percentage of dead cells to their total number. This was done through the ToxiLight_BioAssay Kit, which measures the adenylate kinase enzyme released upon cell death (Fig. 3).

On day 1 of culture, all CNTs performed similarly across all concentrations, with all cytotoxicities below 10%. Hence, short-term contact did not induce excessive cell death, regardless of the CNT surface chemistry used in this study. This suggests that the initial reaction of macrophages is governed by other physicochemical properties – such as CNT shape and size, and their tendency to agglomerate. All of the functionalized CNTs shared similar dimensions, while uCNTs were longer and had the highest tendency to agglomerate (ESI 1†). The latter reduced the effective area of cell – uCNT interactions, likely resulting in lower short-term cytotoxicity.

At longer culture times, higher selectivity towards certain surface chemistries was observed. uCNTs, HO, and HNH had similar cytotoxicities at <20% across all concentrations. For HO and HNH, this is possibly due to high dispersibility, low aspect ratios, reduced stiffness, and high amounts of surface functional groups, all of which are expected to facilitate phagocytosis and reduce overall CNT toxicity.[3,31] Facile internalization has been suggested to promote the *in vitro* biodegradation of CNTs, which is governed by oxidative stress in macrophages.[32,33] In contrast, the low cytotoxicity observed for the uCNTs is probably due to their tendency to agglomerate, which reduces the effective surface area-to-volume ratio.[34]

Meanwhile, LO and LNH were found to be more cytotoxic towards macrophages at concentrations above 25 μg mL^{-1} (LO) or equal to 75 μg mL^{-1} (LNH) and during longer culture times (3 days). Following the trend observed for the number of cells (Fig. 2), LNH appeared benign at lower concentrations (around 10% at 25 and 50 μg mL^{-1}), reached a cytotoxicity of 26% at 75 μg mL^{-1}, and dropped back to 12% at 100 μg mL^{-1}. The secondary drop in cytotoxicity might be due to CNT's secondary agglomeration, but an unequivocal explanation is impossible in the current study. For LO, cytotoxicity reached 30% at concentrations as low as 25 μg mL^{-1} and exceeded 40% at higher concentrations. Hence, both the LO and LNH were cytotoxic to macrophages – LO at all concentrations and LNH – at 75 μg

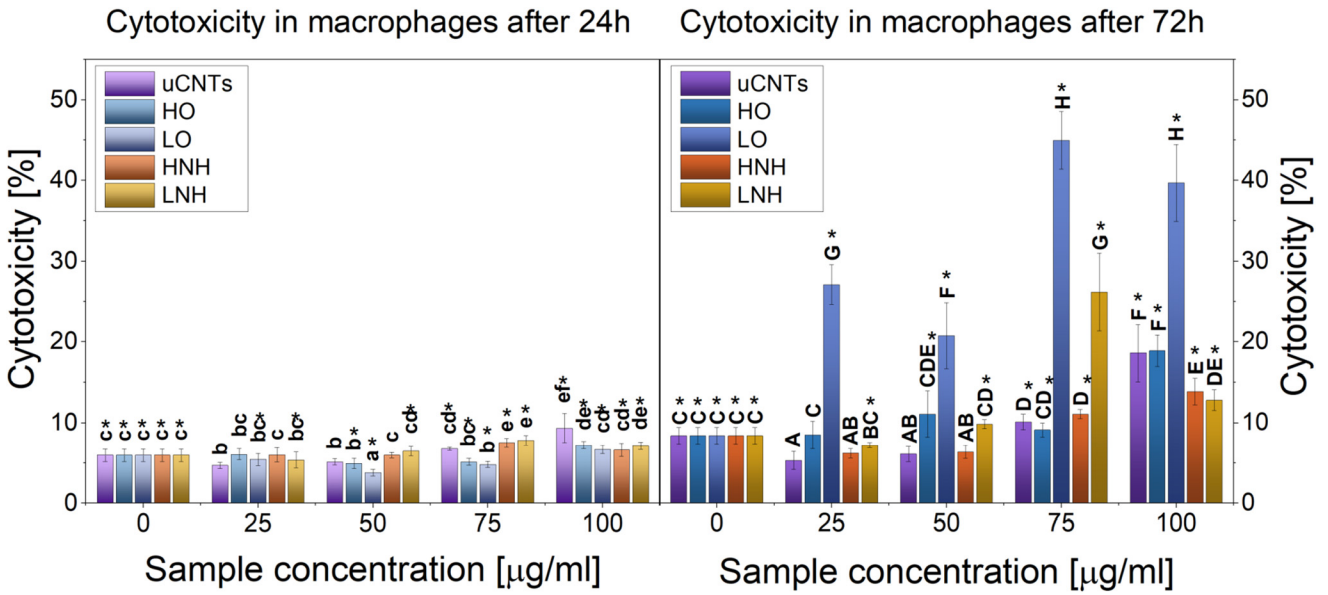

Fig. 3 RAW 264.7 murine macrophage cytotoxicity toward CNTs, tested *via* the ToxiLight assay. The data are presented as means ± SD. Statistically significant differences ($p < 0.05$) between the tested materials compared to one another are marked a–e for the 1st day of culture and A–H for the 3rd day of culture; * indicates statistically significant differences between day 1 and day 3 of culture.

mL^{-1}. Because all of the functionalized CNTs used in this study had similar dimensions, differences in cytotoxicity should be attributed solely to the chemical species present on their sidewalls. These govern the mechanisms of material recognition and internalization by cells, as well as affects the impact on cellular organelles (such as lysosomes) after entering cells. It also known to affect the cellular biodegradation.[32,33] At day 3, the cytotoxicity results align with the data for the total number of macrophages (Fig. 2), wherein LO caused a significant reduction in macrophage number. At the current stage, it is hard to judge why the uCNTs did not present significant cytotoxicity towards macrophages. However, similar results have already been reported. For example, Vittorio *et al.*[35] reported higher viability of human neuroblastoma cells when in contact with unfunctionalized CNTs, as compared to slightly oxidized materials. In the literature, various contradictory results on this matter can be observed, with some studies suggesting better cytocompatibility of the sedimented, unfunctionalized CNTs, as compared to their well-dispersed derivatives.[36] It is our opinion that this arises from the fact that there are numerous factors affecting CNT cytocompatibility, while not all of the studies specifically analyzed cell viability. When considering nanomaterials with high innate cytotoxicity, agglomeration and sedimentation leads to decreased area of cell–material interactions, thus also decreasing their apparent cytotoxicity effects. However, an opposite trend is expected when considering *in vivo* applications, wherein agglomeration increases a materials retention in tissues, possibly leading to adverse prolonged reactions.[37]

Interestingly, similar to our previous studies, where CNTs were administered as layers or inside the CNFs, cytotoxicity was not correlated with ROS production (Fig. 4). Regardless of surface chemistry, all CNTs caused an increase in ROS production on day 1 of culture. In all cases, the values showed a slight positive correlation with CNTs concentrations. For the functionalized CNTs, an up-production of ROS on day 1 exceeded 300% of the control (no CNTs present) and was comparable to the values found by Elgrabli *et al.*[33] Meanwhile, on day 3, ROS production dropped below 200% for the 100 μg mL^{-1} concentration and below 100% for the 25 and 50 μg mL^{-1} concentrations. This indicates that short, well-dispersible, and highly functionalized CNTs induce oxidative stress in macrophages during short-term cultures. This effect is alleviated when cellular contact with CNTs is prolonged. As suggested by Elgrabli *et al.*,[33] degradation of functionalized CNTs proceeds after 24 h of culture, which might indicate that only initial cellular contact is associated with ROS production. In contrast, the later steps proceed without ROS participation.

On the other hand, in the case of uCNTs, a significantly higher production of ROS across all concentrations, regardless of culture time, was observed. Specifically, at the 25 μg mL^{-1} concentration, recorded ROS values were 960% on day 1 of culture and 150% on day 3 – a similar reduction trend at longer culture times (albeit much larger) to the functionalized CNTs. On day 1, an up-production of ROS (up to 18 000%) didn't correlate with CNT concentration, but this changed on day 3, which was directly proportional to the increasing concentration of uCNT (up to 45 000%). In a study by Kagan *et al.*,[38] lung macrophages were found to initiate the extracellular digestion of single-walled CNTs *via* superoxide/peroxynitrite oxidative pathways. These mechanisms were positively correlated with ROS production. Because uCNTs are prone to agglomerate and hence are less likely to be phagocytosed and degraded inside macrophages, the macrophages may thus be

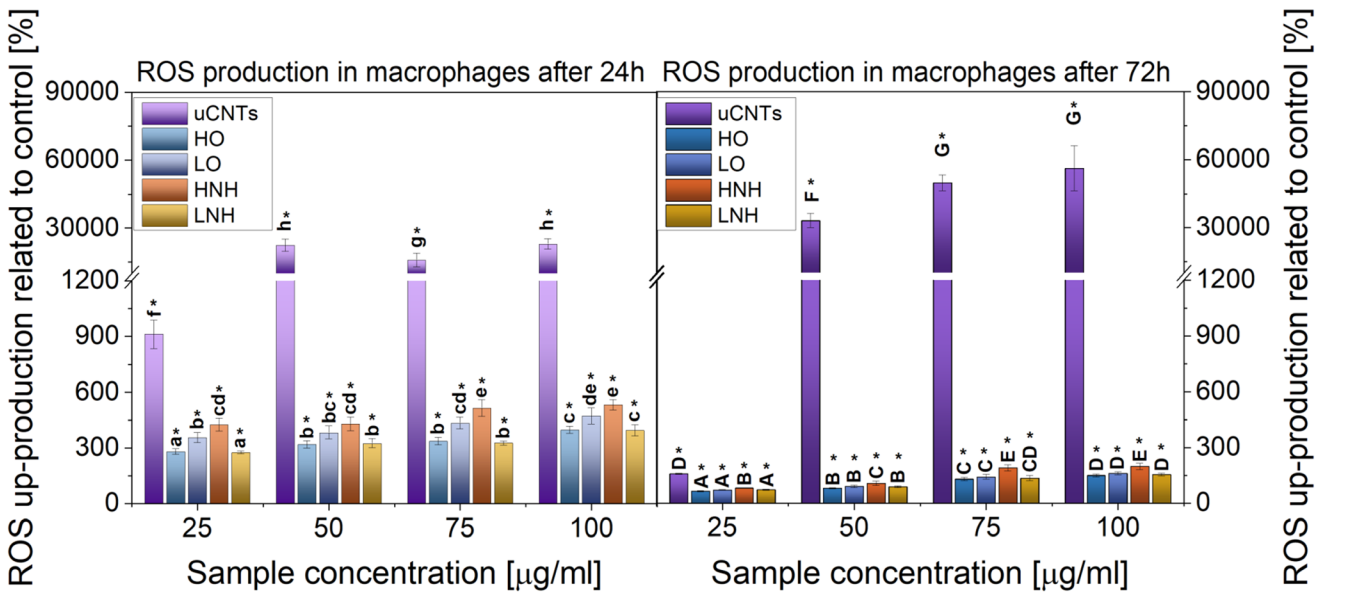

Fig. 4 ROS production in RAW 264.7 macrophages cultured with CNTs, evaluated *via* DCFH-DA. The data are presented as means ± SD. Statistically significant differences ($p < 0.05$) between the tested materials compared to one another are marked a–h for the 1st day of culture and A–G for the 3rd day of culture; * indicates statistically significant differences between day 1 and day 3 of culture.

forced to initiate another mechanism that could cause their clearance – *i.e.*, extracellular degradation. Because uCNTs are non-functionalized (*i.e.*, fewer structural defects and thus increased stability), their degradation is prolonged compared to functionalized CNTs. Because they are less likely to be internalized, the ROS up-production lasts much longer. Based on the literature data, ROS production is expected to persist beyond 200 h.[33,38] Still, it is important to note that in this case, an up-production of exogenous ROS is not cytotoxic to macrophages (Fig. 3).

3.2.2. Cell observation *via* electron microscopy. Upon culturing with 50 μg mL^{-1} of CNTs in the medium for 7 days, scanning electron microscopy observations revealed differences in cell number, size, and morphology (Fig. 5). Some trends toward specific size and shape adaptations could be identified for different functional groups present on the CNT sidewalls. For the control, macrophages were attached, flattened, and spread onto the surface. Similar morphology was also observed in contact with untreated carbon nanotubes (uCNTs) (Fig. 5A–H). This is in line with the cytotoxicity results (Fig. 3). As already suggested, uCNTs have the highest tendency to form agglomerates. Such agglomerates may reach the microscale, reducing the overall surface area-to-volume ratio, diminishing the effective area of cell–material interactions. This might have contributed to the visibly unaltered morphology of macrophages in contact with uCNTs. In contrast, with the functionalized CNTs the macrophages grew larger, which might be a hallmark of CNT internalization.

Among the functionalized CNTs, the most significant differences were seemingly governed by the CNT oxidation states. The lowest number of macrophages was observed for the HO and HNH samples (Fig. 5I and Q), and they were oval-shaped or elongated, with a considerable number of filopodia (Fig. 5K, L, S and T), and visibly smoother surfaces (Fig. 5L and T). Higher amounts of larger and more round cells with rougher surfaces were found upon culturing with LO and LNH (Fig. 5M and U). Changes in macrophage morphology could be caused by better dispersibility of HO and HNH, as compared to LO

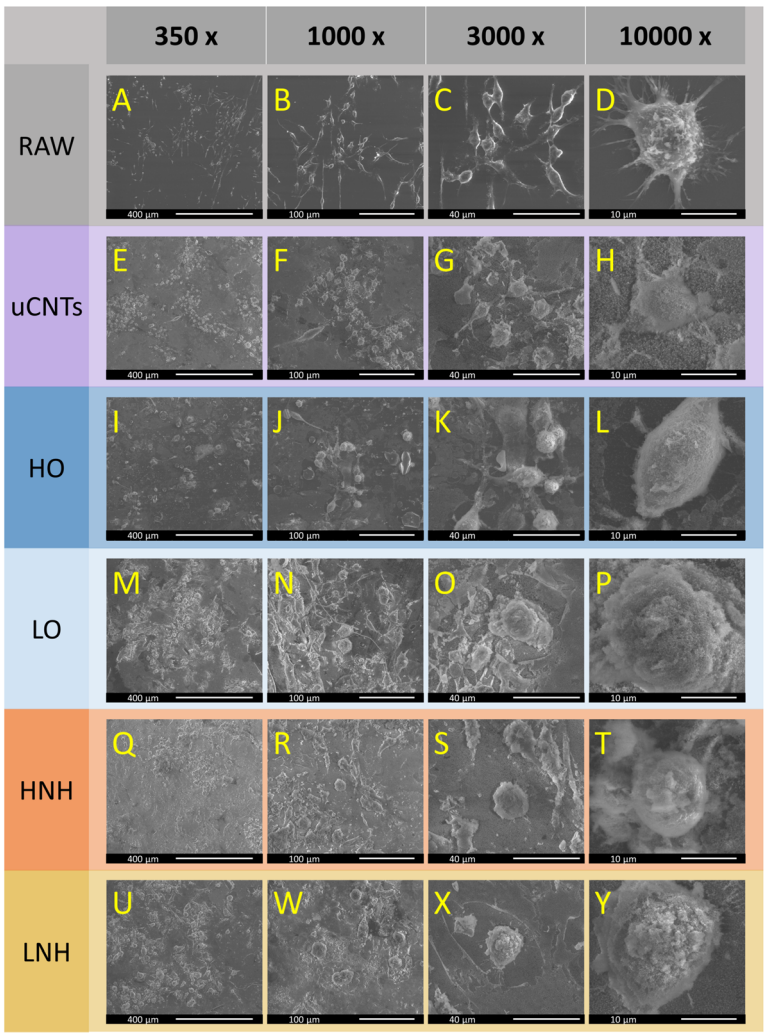

Fig. 5 Scanning electron images of the macrophages and their morphological changes at the end of day 7 of culture with CNTs at a 50 μg mL^{-1} concentration.

and LNH.[19] When CNTs form small aggregates, macrophages can become entangled with them during cell culture, making the cell surface visibly rougher (Fig. 5P and Y). This phenomenon was confirmed through TEM images, wherein cells were surrounded by the LO and LNH CNTs (ESI 9†). Because HO and HNH are short and highly dispersible, their effective phagocytosis is facilitated.[3] Hence, they are not present on the cell surface, so the cell walls remain smooth. In HNH, the cells were more rounded than in HO, with some elongated cells still noticeable (ESI 8†).

TEM images suggested that the CNTs were able to penetrate the cells *via* passive transport and phagocytosis (Fig. 6: orange and yellow arrows, respectively), with cell appendages visibly scraping the CNTs (Fig. 6c). Using SEM, Krysko *et al.*[39] studied the surface characteristics of macrophages upon being cultured with apoptotic or necrotic fibroblasts. Macrophages which internalized the apoptotic cells *via* phagocytosis were characterized by rounded surface protuberances. Meanwhile, macrophages that internalized the necrotic cells likely *via* micropinocytosis had irregular, ruffled membranes, with small protrusions visible. The latter were also observed in the case of LO and LNH CNTs (Fig. 5M–P and U–Y). It can, thus, be suggested that CNTs which are better dispersed and have a higher share of carbon atoms at a +3 oxidation number, can undergo both an active phagocytosis as well as passive diffusion. Meanwhile, CNTs that are more prone to aggregate, and have lower amounts of carbon atoms at a +3 oxidation number, enter the cells less effectively, leading to a mechanism that might be micropinocytosis.

Modifications of CNTs with functional groups increase their dispersability and facilitate their penetration into a cell. We found that this process was more effective for the HO and HNH samples. Being short and highly dispersible, HO and HNH can easily penetrate the cell wall (either passively or actively), as already suggested in various studies.[3,40] LO and LNH, which had slightly different surface chemistry and higher tendency to agglomerate (ESI 1† and Benko *et al.*[19]), are less likely to penetrate the cell walls. This phenomenon can be observed in ESI 9,† wherein LO and LNH were mostly present outside the cells, tightly surrounding the cell wall and likely reducing cell viability by isolating it from its surroundings (as observe in the cytotoxicity studies – in general, LO and LNH were found to induce higher cytotoxicity as compared with HO and HNH, Fig. 3). Length, diameter, surface modification, purity, and structural defects of CNTs are important factors that influence macrophage morphology. So many governing factors may lead to high discrepancies in the literature, and the impact of different features may be contradictory. Nagai *et al.*[41] proved that the diameter and crystallinity of MWCNTs are critical factors responsible for mesothelial cell injury. ~50 nm thin and highly crystalline MWCNTs pierced the mesothelial membranes of RAW macrophages, whereas thicker MWCNTs (~150 nm) could not penetrate the cellular membrane and injure mesothelial cells. In our study, MWCNTs with diameters between 10 and 50 nm did not cause significant injury to cells, which is in contrast to the cited study. Likely, this is due to the fact that our CNTs are much shorter and less crystalline (*i.e.*, have more structural defects from introducing oxygen atoms). Liu *et al.*[42] indicated that MWCNTs induce cytotoxicity in a length- and cell-type-dependent manner. Longer MWCNTs (3 to 14 μm) exerted higher cytotoxicity, especially in contact with RAW264.7 cells, while shorter (1.5 μm) MWCNTs were significantly less cytotoxic. Our materials have lengths comparable to the latter, yielding similar results. Functionalization of MWCNTs is also an important factor influencing macrophage morphology. Gasser *et al.*[43] observed that functionalization of MWCNTs with polar groups (–COOH, an $–NH_2$) resulted in higher cytotoxicity, higher induction of a TNF-α secretion (by $–NH_2$), higher LDH release (by $–NH_2$), increased antioxidant glutathione depletion (by $–NH_2$ and –COOH), and increased cell apoptosis (by –COOH). These results contradict our findings, but understanding the discrepancies is impossible because the authors of the cited study did not show any results of the CNTs' physicochemical properties. Because CNT dimensions and chemical compositions are unclear, one cannot explain the mechanisms of the observed phenomena. Zhang *et al.*[44] noticed that well-dispersed MWCNT–COOH were internalized by RAW264.7 cells more efficiently. At the same time, the more dispersed but neutrally charged MWCNT–PEG, had difficulty

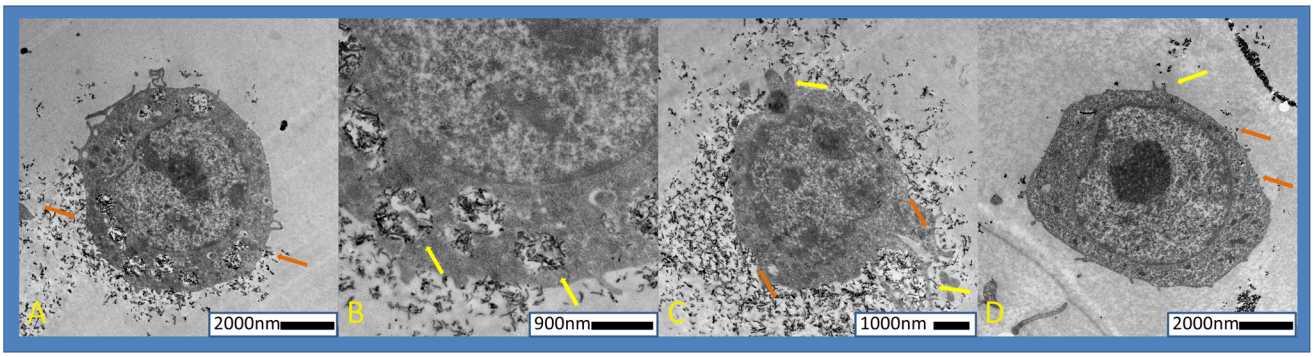

Fig. 6 Transmission electron images of macrophages and their interactions with CNTs. (A–C) HO, (D) HNH. Orange arrows – passive transport, yellow arrows – phagocytosis.

entering the cells and formed agglomerates that seemed to densely cover the cell surface. This result agrees with our study, wherein CNTs with a higher tendency to form agglomerates (LO and LNH forms) were observed outside of the cells. At the same time, highly dispersible HO and HNH could be found inside the macrophages (Fig. 6). In another study, Jiang *et al.*[45] compared PEG and COOH-functionalized MWCNT. In that case, MWCNT–COOH were better internalized by RAW264.7 cells and rat peritoneal macrophages. Acid functionalization caused a greater reduction in cell viability and elicited higher NADPH oxidase activity and ROS generation, causing more pronounced cell apoptosis. Again, the physicochemical analysis shown in that study is insufficient to compare the published results with the ones presented for our materials – especially, dispersibility and dimensions were not studied. Further, the relative amount of oxygen atoms and the resultant XPS spectra were not shown for assessing chemical composition.

All in all, taking into account our results, as well as those described in the literature, there seems to be a consensus that a higher share of the negatively charged functional groups (HO and HNH) improves CNT dispersion, reducing their tendency to form agglomerates (ESI 1† and Benko *et al.*[19]), thus improving their internalization by macrophages. On the contrary, MWCNTs that contain carbon with a lower oxidation number in their structure, having less negative (LO and LNH) or neutral surface charge (uCNTs), have difficulty entering cells, causing increased cytotoxicity in macrophages (Fig. 3).

3.2.3. Cytocompatibility with HDF cells. As reported, uCNTs tend to agglomerate, sediment, and boost ROS production. As such, they were rejected from further studies as susceptible to yielding false positive or false negative results, especially in colorimetric assays. Instead, studies concerning normal human dermal fibroblasts, melanoma cells, and bacteria were conducted only on functionalized CNTs to reveal the effects that different surface chemistries evoke on the cells.

When examining the samples with different degrees of functionalization, differences in HDF proliferation were observed (Fig. 7, different presentations of the same data can be found in ESI 10†). In short-term cultures (24 h), HO was found to reduce the number of cells the most (by 80%). Interestingly, this reduction was similar regardless of the HO concentration. All the other CNTs also caused a reduction in the number of cells but to a much smaller extent (30% in LO, 35% in LNH, and 63% in HNH). In the case of HNH, cell number almost linearly decreased with increasing CNT concentration. For LO, cell number remained almost constant up to 75 μg mL^{-1}, and then dropped at 100 μg mL^{-1}. For LNH, the number of cells only slightly decreased between different concentrations. It is, therefore, apparent that HO and HNH are more detrimental to HDF cells at shorter culture times – a trend not observed in cultures with macrophages. However, this trend was no longer visible at longer culture times, wherein all the CNTs appeared to support cellular proliferation to some extent.

On day 3 and across all concentrations, the number of cells was the highest for HO, followed by LO, HNH, and LNH samples. In all samples, the biggest decrease in cell number was at the 50 μg mL^{-1} concentration. For HNH and LNH, a further increase in CNT concentration did not significantly alter cell number, while the same was slightly increased in the case of HO and LO. No clear correlation between the dosage and the number of cells might indicate that the materials slightly handicapped cellular proliferation, possibly by affecting initial cell adhesion, albeit no obvious cytotoxic effect is suspected. It is also possible that at the initial contact,

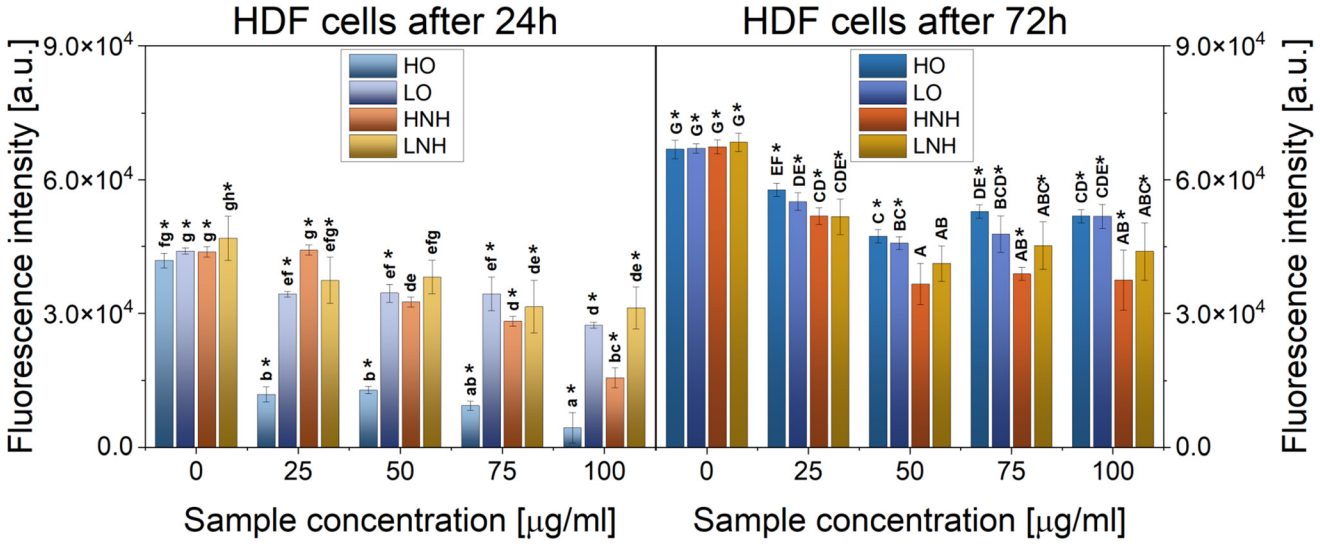

Fig. 7 Proliferation of human dermal fibroblasts cultured with increasing concentrations of the modified CNTs. The data are presented as means ± SD. Statistically significant differences ($p < 0.05$) between the tested materials compared to one another are marked a–h for the 1st day of culture and A–G for the 3rd day of culture; * indicates statistically significant differences between day 1 and day 3 of culture.

the cells were preoccupied with the CNTs phagocytosis, reducing their proliferation. Because on day 1 the number of cells for the HO treatment was the lowest, the fact that it reached values like the rest of CNTs on day 3 indicated the highest growth kinetics, suggesting that these CNTs are, in fact, not cytotoxic at longer culture times. A possible explanation of this phenomenon is that the most negative overall surface charge characteristics of these CNTs likely caused the strongest interaction with the cell membrane. This, in turn, might have affected cellular adhesion, possibly retarding it. Because HDFs are anchorage-dependent cells, futile adhesion leads to cell death, fewer cell-to-cell contacts, and mitigated proliferation. It can be hypothesized that live cells that managed to adhere to the cell well bottom then proceed with the CNTs intake, reducing their effective amount in culture media, and diminishing their negative effect on the adhesion and spreading. If the materials were toxic, fewer cells would have also been observed at longer culture times, as those that adhered to the surface would also be killed. It can thus be suggested that HO is not cytotoxic under the conditions of this study – once the cells adhere to the surface of the well, they can effectively increase in number. Similar results were already reported in our previous study, wherein a retarded adhesion of HDF cells was observed on HO-modified carbon nanofibers. However, the same fibers were found to support cell growth at longer culture times.[18] A higher number of cells at day 3 of culture with HO, compared with HNH and LNH, indicated that HO is more cytocompatible than the amidized samples.

Meanwhile, the cytocompatibility of LO was similar to that of HO. Both of these materials may be concluded as cytocompatible, regardless of concentration, as at the highest concentration of 100 μg mL^{-1}, the number of viable cells was 77% at day 3 of culture. At the same time, the HNH and LNH may be considered slightly cytotoxic at 100 μg mL^{-1}, as the number of cells dropped to 56% and 64%, respectively. It can thus be suggested that at longer culture times, HDF cells prefer CNTs with mostly oxygen-based functional groups, as compared to amine or amide groups.

3.2.4. Anti-cancer cell performance. When different CNT samples were exposed to melanoma cells, a clear dose-dependent cytotoxic pattern was observed, especially noticeable for the LO and LNH samples (Fig. 8, a different presentation of the same data can be found in ESI 11†), and this effect was more pronounced at day 1 of culture. The anticancer behavior was still significant but less prominent in HO and HNH samples. A stronger reaction was found for the case of HO, with more significant changes found on day 1 of culture and with increasing concentration. Meanwhile, for HNH, a reduction in melanoma cell number was observed at the 25 μg mL^{-1} concentration, and it did not further increase at longer culture times or across increasing concentrations.

CNTs have been extensively studied as drug-delivery vehicles for chemotherapy and anticancer drugs. However, their direct antitumoral effect has not been widely reported. Different studies have found that functionalized carbon nanomaterials can be used as drug delivery vehicles, photothermal materials, or as photodynamic therapy agents while remaining safe towards normal healthy cells.[2] It has been reported that the toxicity of CNTs in tumor cell lines increased when carboxyl and hydroxyl groups were present on their surface.[46] A different study found that COOH-functionalized CNTs have higher clastogenic and genotoxic potential than non-functionalized CNTs.[47] This study found that CNTs of similar shapes and sizes, but slightly differing in the type of the major func-

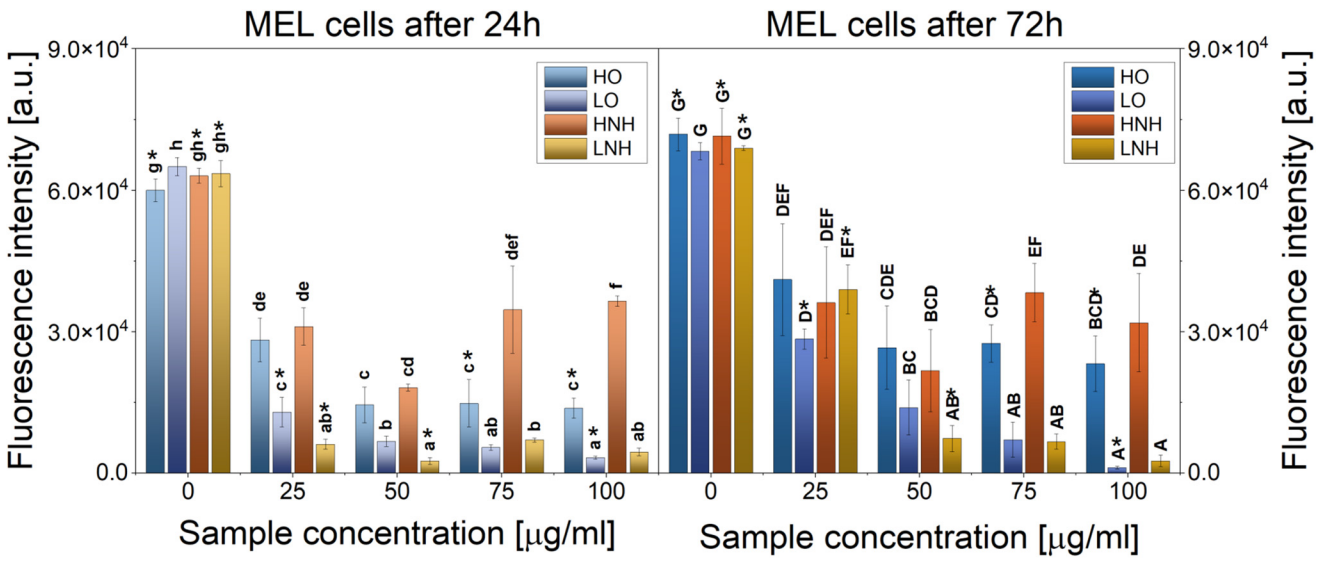

Fig. 8 Proliferation of melanoma cells cultured with increasing concentrations of the modified CNTs. The data are presented as means ± SD. Statistically significant differences ($p < 0.05$) between the tested materials compared to one another are marked a–h for the 1st day of culture and A–G for the 3rd day of culture; * indicates statistically significant differences between day 1 and day 3 of culture.

tional groups at their sidewalls, induce different cytotoxic and anticancer reactions. Specifically, CNTs with the majority of +2 oxidation number carbon atoms (LO and LNH) were found to be more effective in killing cancer cells than the CNTs also having carbon atoms at +3 oxidation number (HO and HNH). In the latter case, oxygen-based functional groups were more effective than the nitrogen-modified ones. At the same time, the LO sample was also the most detrimental to macrophages, followed by LNH.

We believe that the enhancement of *in vitro* anticancer efficiency observed here was caused by the specific surface chemistry, combined with high aspect ratio and high surface area of the CNTs. This provided multiple adhesion sites to cells, leading to effective cell interactions, possibly penetration, and killing.[48] Once attached to the cells, LO and LNH likely isolated them from their surroundings, thus leading to death. However, there must be some additional mechanism at play here, as HO and HNH, which were safe to macrophages (Fig. 3) and HDF cells (Fig. 7), were also able to effectively target melanoma cells. Cell number reduction was up to 80% in HO at day 1, and at concentrations between 50 and 100 μg mL^{-1}, and up to 70% for HNH at a 50 μg mL^{-1} concentration, regardless of culture time. Hence, a chemical modification that leads to the formation of carbon atoms at a +3 oxidation appears to be a route to obtaining improved carriers for anticancer drug therapy, which are not only safe to the healthy cells, but also are able to reduce the number of cancer cells in the culture, without using any exogenous factors. We think that for the LO and LNH, at least two cancer cell-killing mechanisms were at play, namely ROS overproduction and physical isolation of cells from their surroundings. The latter can also affect the healthy cells. For HO and HNH, cellular penetration was more likely, hence, the cell wrapping mechanism was not present. However, these CNTs could also induce an overproduction of ROS. In order to confirm this hypothesis, ROS production in melanoma cells was evaluated.

3.2.5. Reactive oxygen species (ROS) production in melanoma cells. The mechanism of toxicity towards melanoma cells was evaluated by analyzing the reactive oxygen species (ROS) induced in melanoma cells upon a 24 h exposure to increasing CNT concentrations (25, 50, 75, and 100 μg mL^{-1}). The results (Fig. 9) showed a slight increase in ROS production when the CNTs were present in the media, with a dose-dependent effect. Similar to macrophages, melanoma cells up-produce ROS in contact with functionalized CNTs, but to a much smaller extent (up to 160% as compared with up to 520% on day 1 of culture, both recorded for HNH). Similar to macrophages (Fig. 4), for melanoma cells, HNH showed the highest ROS up-production, while HO and LNH showed the lowest (Fig. 9). Again, there is no obvious correlation between the ROS production and cytotoxicity (Fig. 3). Specifically, the highest production of ROS was observed for HNH, followed by LO, LNH, and HO. Meanwhile, HO and HNH were found to be the least efficient in targeting the cancer cells. As already mentioned, LO and LNH are suggested to have two cancer cell killing mechanisms at their disposal – they isolate the cells

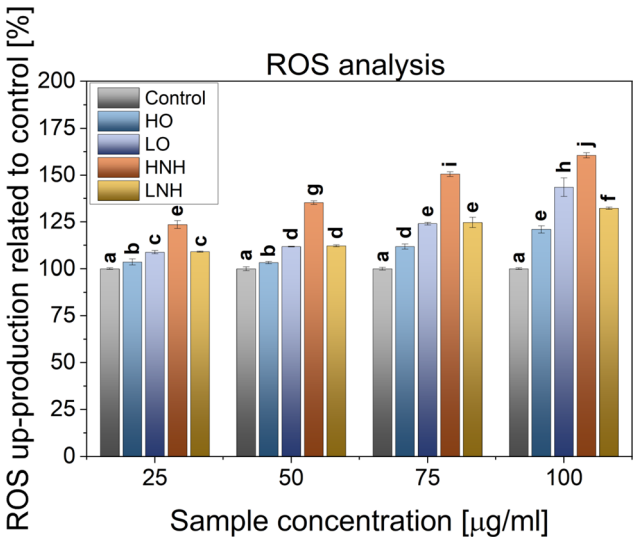

Fig. 9 ROS analysis in melanoma cells subjected to an increasing concentration of different samples. The data are presented as means ± SD. Statistically significant differences ($p < 0.05$) between the tested materials compared to one another are marked a–j for the 1st day of culture.

from their environment and cause ROS up-production, but isolation can also affect the healthy cells, so these mechanisms are far from perfect. On the other hand, ROS-related therapies are in general far safer for healthy cells, as these cells possess more efficient antioxidant systems to balance the exogenous ROS.[49] At the same time, cancer cells have higher levels of endogenous ROS and their antioxidant systems to balance the exogenous ROS are often depleted.[50] Hence, HO and HNH, which likely do not induce contact-killing mechanism and lack highly desired selectivity, are still able to target the cancer cells with more selective, ROS-related killing. We believe that because HO and HNH can easily translocate through the cellular membrane, not only do they induce exogenous ROS, but also endogenous ROS, resulting in an efficient cancer cell killing mechanism, while still being safe to normal, healthy cells. Importantly, similar effects were also observed where the same CNTs were presented to cells as cell culture scaffolds.[17] It cannot be excluded that more mechanisms are at play here, including the CNTs' electro-donor properties, or side groups sizes and charges. A more detailed study should be conducted to investigate the contribution of these mechanisms and the relationship or synergy with different physicochemical properties of the CNTs.

3.2.6. Antimicrobial activity. Colony-counting unit assays were conducted using MDR *Escherichia coli* and MRSA bacteria (Fig. 10, different presentations of the same data can be found in ESI 12 and ESI 13†) to evaluate the antibacterial properties of the different CNTs. As can be seen, a dose-dependent inhibition was found when the four samples were exposed to MDR–EC and MRSA, producing significant statistical differences compared to the controls, even at the lowest concentration in the range tested.

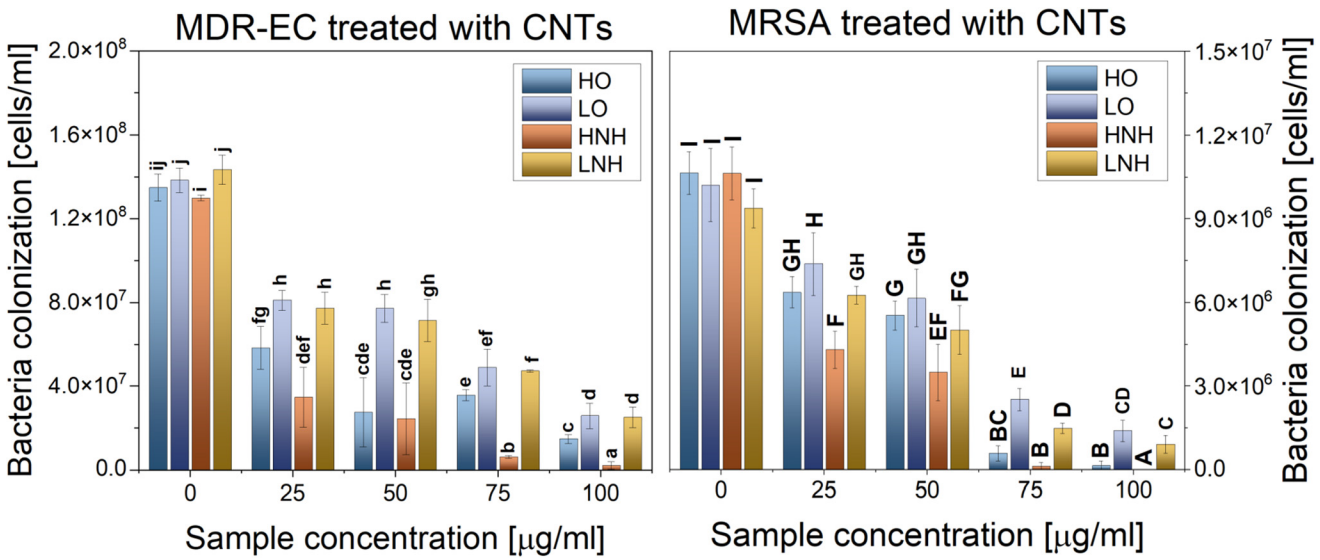

Fig. 10 Antimicrobial properties of CNTs against MDR–EC and MRSA, as a function of increasing concentration. The data are presented as means ± SD. Statistically significant differences ($p < 0.05$) between the tested materials compared to one another are marked a–j (MDR–EC) and A–I (MRSA).

The strongest antibacterial effect against the Gram-negative *E. coli* was observed for HNH, followed by HO, LNH, and LO. In our previous studies, similar results were observed when the same bacteria were directly seeded on the all-CNTs layers[17] or CNT modified fibers.[18] Hence, MDR–EC are suggested to be highly sensitive toward CNT surface chemistry, wherein carbon atoms with a +3 oxidation number, resulting in larger and more polar groups, are detrimental, and a successive modification with ammonia further boosts this effect.

When Gram-positive bacteria (MRSA) were exposed to different CNTs, moderate inhibitions were observed up to 50 μg mL^{-1}, and a much stronger inhibition was found at the 75 and 100 μg mL^{-1} concentrations. Despite a stronger inhibition observed for the MRSA at higher concentrations, overall, a more sustained and efficient antimicrobial behavior was found against the Gram-negative strain MDR *E. coli*, following the trend observed in similar studies.[51] For MRSA, the same susceptibility as already observed in MDR–EC towards the CNT chemical composition was observed, with HNH being the most detrimental (followed by HO) and LO – the least.

In our previous studies, the same trend was also observed when CNTs were embedded inside carbon nanofibers, but when in contact with CNT layers, stronger antibacterial effects against MRSA were recorded for both types of amidized samples (HNH and LNH). Thus, it seems that when CNTs are not able to penetrate the bacteria, their antibacterial effect is mainly governed by their work function values and surface chemistry. Meanwhile, when CNTs are well dispersed in cell culture liquid, different determinants of their antibacterial properties are expected, apart from surface chemistry and electro-donor properties, also including electrostatic repulsion, contact killing and/or ROS production. As already suggested for cancer cells, LO and LNH might induce toxicity of different cells and bacteria by wrapping them and isolating from their surroundings. Whether this could happen for the negatively charged bacteria is debatable because all the CNTs used in this study were negatively charged,[19] and thus electrostatic repulsion should mitigate the wrapping. Similarly, bacteria membrane penetration expected for the HO and HNH, could be mitigated by the same effect. However, in the closed and limited cell well environment, electrostatically repulsive materials can still induce bacteria death,[1] and the contact killing mechanisms cannot be entirely excluded. Furthermore, bacteria are also more susceptible toward ROS therapies than mammalian cells because they completely lack any antioxidative system.

The antibacterial enhancement with increasing CNT concentrations might also be explained by considering the bacteria membrane-piercing effect. It was previously reported that CNT toxicity is affected by the dispersity and conformation of CNTs because of increased bacteria-contact opportunities.

To sum up, the antibacterial properties might be explained by: (1) electrostatic repulsion, (2) cell membrane damage by direct contact between the CNTs and bacteria, and (3) a slight overproduction of ROS. In agreement with our previous studies, this universal antibacterial effect, regardless of the bacterial strain and the CNT concentration, was observed for the HO and HNH samples, characterized by better dispersibility and higher shares of carbon atoms at +3 oxidation numbers. Hence, these CNTs are characterized by a similar performance with cells and pathogens regardless of the form of contact – whether as layers, matrix additives, or administered in free-form, these CNTs are cytocompatible while still being able to effectively eradicate bacteria and kill cancer cells, at least under the conditions of this and previous studies.[17,18]

Table 3 A summary of CNT properties reported in this and previous study [19]

	HO	LO	HNH	LNH
Oxygen content [%]	18.8±1.2	13.7±2.8	15.5±1.5	9.5±6.7
Nitrogen content [%]	0	0	2.9±.0.3	1.6±1.1
C–C, C–O, C–N bonds [%][19]	19.5	29.5	15.8	18.5
C═O bonds [%][19]	29	18.1	20.5	16.7
Length range [nm][19]	100–800	100–1200	100–800	100–1200
Diameter [nm][19]	10–50			
Cytotoxicity with RAW 264.7 (day 3, 75 μg mL^{-1})	9%	45%	11%	26%
Cytotoxicity with HDF (day 3, 75 μg mL^{-1})	21%	29%	42%	34%
Cytotoxicity with MEL (day 3, 75 μg mL^{-1})	59%	89%	43%	90%
Reduction of MDR–EC bacteria colonization (75 μg mL^{-1})	74%	65%	95%	67%
Reduction of MRSA bacteria colonization (75 μg mL^{-1})	95%	75%	99%	84%

This study provides a useful guidance for designing new types of safe CNT delivery vehicles that can effectively target cancer cells and bacteria while being safe to healthy cells.

4. Conclusions

This study was designed to verify how different surface chemistry modifications can affect the functional performance of CNTs administered to cells in free form (*i.e.*, as it would be for their application for drug delivery purposes). To do so, four types of functionalized CNTs (HO, LO, HNH, and LNH) were tested along with their unmodified precursor. A summary of an objective selection of some of the most important findings of this study is gathered in Table 3. We found that minute changes in the chemical composition greatly affected the biological performance of the tested MWCNTs. When macrophages were cultured for 3 days with LO (low oxidized CNTs), a cytotoxicity of 45% was recorded. The same concentration reduced the number of melanoma cells by 90%. A DCC-activated reaction with ammonia that yielded LNH reduced the cytotoxicity to 26% while maintaining similar efficiency against melanoma cells. At the same time, a 75 μg mL^{-1} concentration of both LO and LNH reduced bacterial colonization by 65% (MDR–EC) or 75–85% (MRSA). Hence, the presence of a high share of carbon atoms at a +2 oxidation number constitutes cytotoxic CNTs which are also antibacterial. Cytocompatibility can be improved by a seemingly marginal change that leads to the introduction of 2% m at of nitrogen atoms. This is an important guidance for anyone working with CNTs for biological applications, as OH-functionalized CNTs are among the most popular commercially available products.

At the same time, when CNTs were rich in carbon atoms at a +3 oxidation number (HO), their cytocompatibility was natively higher. This is because these CNTs do not wrap cells, isolating them from their surroundings. Instead, they can easily translocate through the cellular membrane and can thus be regarded as interesting candidates for targeted intracellular drug delivery. At the same time, high anticancer performance, combined with universal and high antibacterial properties, were recorded here. Thus, HO appears to possess a perfect combination of features that are highly desirable from the biomedical point of view. Interestingly enough, these positive qualities can be even further boosted by subjecting these CNTs to the DCC-activated amide modification. Again, a slight change in the chemical composition which yielded materials with 2% m at of nitrogen, led to an improvement in cytocompatibility, anticancer properties, and antibacterial effects. This study proves that the biological properties of CNTs are governed by their surface chemistry. Having similar ROS production efficiency and different mechanisms against different cell types could be explained by CNT interactions with cell walls. If the CNTs are able to easily penetrate healthy cells, they could be cytocompatible to healthy cells and cytotoxic to ROS-sensitive cells (cancer cells) and organisms (bacteria). At the same time, when CNTs wrap the cells and isolate them from their environment, killing efficiency will be higher, but less selective – *i.e.*, normal healthy cells will also be affected.

Data availability

The raw data required to reproduce these findings will be made available upon request sent directly to the corresponding author.

Author contributions

Aleksandra Benko: Conceptualization, methodology, investigation, resources, data analysis and visualization, funding acquisition, project administration, supervision, writing – original draft preparation, writing – review & editing, proofreading. David Medina-Cruz: Antibacterial, ROS, MEL, and HDF cells experiments, results visualization, writing – proofreading. Sebastian Wilk: preparation of carbon nanotubes. Magdalena Ziąbka: investigation (SEM analysis of cells and their visualization), writing – macrophages analysis, proofreading. Barbara Zagrajczuk: investigation (conducting the colorimetric assays with macrophages), writing (colorimetric assays methods section), data analysis, statistical analysis. Elżbieta Menaszek: investigation (performing macrophage cultures), resources. Olga Barczyk-Woźnicka: Investigation (performing the TEM analysis of cells), resources. Gregory Guisbiers: Supervision,

proofreading. Thomas J. Webster: Resources, funding acquisition, writing – proofreading, supervision.

Conflicts of interest

There are no conflicts to declare.

Acknowledgements

The authors thank the National Centre for Research and Development (Grant No: LIDER/7/0020/L-11/19/NCBR/2020) for financially supporting this project.

References

1 A. Benko, K. Reczyńska-Kolman, D. Medina-Cruz, J. L. Cholula-Diaz, C. O'Connell, L. B. Truong, L. Martínez, P. Kazimierczak, A. Przekora, S. Wilk, H. Barabadi, Y. Huttel, J. M. García-Martín, E. Pamuła and T. J. Webster, in *Antimicrobial Activity of Nanoparticles*, ed. G. Guisbiers, Elsevier, 2023, pp. 19–67, DOI: 10.1016/B978-0-12-821637-8.00002-X.
2 A. Benko, D. Medina-Cruz, A. Vernet-Crua, C. P. O'Connell, M. Świętek, H. Barabadi, M. Saravanan and T. J. Webster, *Cancer Drug Resist.*, 2021, **4**, 264–297.
3 K. Kostarelos, *Nat. Biotechnol.*, 2008, **26**, 774–776.
4 P. M. Costa, M. Bourgognon, J. T. W. Wang and K. T. Al-Jamal, *J. Controlled Release*, 2016, **241**, 200–219.
5 S.-W. Kim, Y. K. Lee, S.-H. Kim, J.-Y. Park, D. U. Lee, J. Choi, J. H. Hong, S. Kim and D. Khang, *Sci. Rep.*, 2017, **7**, 6454.
6 K. Kostarelos, A. Bianco and M. Prato, *Nat. Nanotechnol.*, 2009, **4**, 627–633.
7 Y. Bai, Z.-H. Huang and F. Kang, *Colloids Surf., A*, 2014, **443**, 66–71.
8 U. Hofer, *Nat. Rev. Microbiol.*, 2019, **17**, 3–3.
9 A. B. Mariotto, K. R. Yabroff, Y. Shao, E. J. Feuer and M. L. Brown, *J. Natl. Cancer Inst.*, 2011, **103**, 117–128.
10 R. L. Siegel, K. D. Miller, H. E. Fuchs and A. Jemal, *CA-Cancer J. Clin.*, 2021, **71**, 7–33.
11 K. Kostarelos, L. Lacerda, G. Pastorin, W. Wu, W. Sebastien, J. Luangsivilay, S. Godefroy, D. Pantarotto, J.-P. Briand, S. Muller, M. Prato and A. Bianco, *Nat. Nanotechnol.*, 2007, **2**, 108–113.
12 G. Modugno, F. Ksar, A. Battigelli, J. Russier, P. Lonchambon, E. Eleto da Silva, C. Ménard-Moyon, B. Soula, A.-M. Galibert, M. Pinault, E. Flahaut, M. Mayne-L'Hermite and A. Bianco, *Carbon*, 2016, **100**, 367–374.
13 K. Bhattacharya, S. P. Mukherjee, A. Gallud, S. C. Burkert, S. Bistarelli, S. Bellucci, M. Bottini, A. Star and B. Fadeel, *Nanomedicine*, 2016, **12**, 333–351.
14 A. Przekora, A. Benko, M. Nocun, J. Wyrwa, M. Blazewicz and G. Ginalska, *Mater. Sci. Eng., C*, 2014, **45**, 287–296.
15 A. Benko, A. Frączek-Szczypta, E. Menaszek, J. Wyrwa, M. Nocuń and M. Błażewicz, *J. Mater. Sci.: Mater. Med.*, 2015, **26**, 262.
16 A. Benko, A. Przekora, A. Wesełucha-Birczyńska, M. Nocuń, G. Ginalska and M. Błażewicz, *Appl. Phys. A*, 2016, **122**, 447.
17 A. Benko, D. Medina-Cruz, J. Duch, T. Popiela, S. Wilk, M. Bińczak, M. Nocuń, E. Menaszek, L. D. Geoffrion, G. Guisbiers, A. Kotarba and T. J. Webster, *Mater. Sci. Eng., C*, 2021, **120**, 111703.
18 S. Wilk, D. Medina-Cruz, M. Zambrzycki, P. K. Szewczyk, M. Nocuń, E. Menaszek, T. J. Webster and A. Benko, *Chem. Eng. J.*, 2022, 140617, DOI: 10.1016/j.cej.2022.140617.
19 A. Benko, J. Duch, M. Gajewska, M. Marzec, A. Bernasik, M. Nocuń, W. Piskorz and A. Kotarba, *Nanoscale*, 2021, **13**, 10152–10166.
20 I. Nanostructured & Amorphous Materials, Amorphous Products | Nanoscale Products - Short MWNT (95+%, OD 10–30 nm), https://www.nanoamor.com/inc/sdetail/4021, (accessed 04.02, 2015).
21 V. Datsyuk, M. Kalyva, K. Papagelis, J. Parthenios, D. Tasis, A. Siokou, I. Kallitsis and C. Galiotis, *Carbon*, 2008, **46**, 833–840.
22 Q. Gu, Y. Ding, Z. Liu, Y. Lin, R. Schlögl, S. Heumann and D. Su, *J. Energy Chem.*, 2019, **32**, 131–137.
23 P. Düngen, R. Schlögl and S. Heumann, *Carbon*, 2018, **130**, 614–622.
24 T. N. Ang, B. R. Young, M. Taylor, R. Burrell, M. K. Aroua, W.-H. Chen and S. Baroutian, *Chemosphere*, 2020, **260**, 127496.
25 Y. Zhao, D. Wu, Y. Chen, Y. Li, X. Fan, F. Zhang, G. Zhang and W. Peng, *J. Colloid Interface Sci.*, 2021, **585**, 640–648.
26 H. Liu, Y. Zhang, R. Li, X. Sun and H. Abou-Rachid, *J. Nanopart. Res.*, 2012, **14**, 1016.
27 S. Rehder, A. Sakmann, T. Rades and C. S. Leopold, *Eur. J. Pharm. Biopharm.*, 2012, **80**, 203–208.
28 V. Datsyuk, M. Kalyva, K. Papagelis, J. Parthenios, D. Tasis, A. Siokou, I. Kallitsis and C. Galiotis, *Carbon*, 2008, **46**, 833–840.
29 D. Roy, N. Tiwari, K. Mukhopadhyay, T. Shripathi and A. K. Saxena, *ChemPhysChem*, 2014, **15**, 3839–3847.
30 M. Worzakowska, M. Sztanke and K. Sztanke, *Int. J. Mol. Sci.*, 2023, **24**, 6190.
31 B. Fadeel and K. Kostarelos, *Nat. Nanotechnol.*, 2020, **15**, 164–164.
32 G. P. Kotchey, Y. Zhao, V. E. Kagan and A. Star, *Adv. Drug Delivery Rev.*, 2013, **65**, 1921–1932.
33 D. Elgrabli, W. Dachraoui, C. Ménard-Moyon, X. J. Liu, D. Bégin, S. Bégin-Colin, A. Bianco, F. Gazeau and D. Alloyeau, *ACS Nano*, 2015, **9**, 10113–10124.
34 A. Nel, T. Xia, L. Mädler and N. Li, *Science*, 2006, **311**, 622–627.
35 O. Vittorio, V. Raffa and A. Cuschieri, *Nanomedicine*, 2009, **5**, 424–431.
36 P. Wick, P. Manser, L. K. Limbach, U. Dettlaff-Weglikowska, F. Krumeich, S. Roth, W. J. Stark and A. Bruinink, *Toxicol. Lett.*, 2007, **168**, 121–131.
37 G. Qu, Y. Bai, Y. Zhang, Q. Jia, W. Zhang and B. Yan, *Carbon*, 2009, **47**, 2060–2069.

38 V. E. Kagan, A. A. Kapralov, C. M. St. Croix, S. C. Watkins, E. R. Kisin, G. P. Kotchey, K. Balasubramanian, I. I. Vlasova, J. Yu, K. Kim, W. Seo, R. K. Mallampalli, A. Star and A. A. Shvedova, *ACS Nano*, 2014, **8**, 5610–5621.
39 D. V. Krysko, G. Denecker, N. Festjens, S. Gabriels, E. Parthoens, K. D'Herde and P. Vandenabeele, *Cell Death Differ.*, 2006, **13**, 2011–2022.
40 N. Chatterjee, J. Yang, S. Kim, S. W. Joo and J. Choi, *Carbon*, 2016, **108**, 529–540.
41 H. Nagai, Y. Okazaki, S. H. Chew, N. Misawa, Y. Yamashita, S. Akatsuka, T. Ishihara, K. Yamashita, Y. Yoshikawa, H. Yasui, L. Jiang, H. Ohara, T. Takahashi, G. Ichihara, K. Kostarelos, Y. Miyata, H. Shinohara and S. Toyokuni, *Proc. Natl. Acad. Sci. U. S. A.*, 2011, **108**, E1330–E1338.
42 D. Liu, L. Wang, Z. Wang and A. Cuschieri, *Nanoscale Res. Lett.*, 2012, **7**, 361.
43 M. Gasser, P. Wick, M. J. Clift, F. Blank, L. Diener, B. Yan, P. Gehr, H. F. Krug and B. Rothen-Rutishauser, *Part. Fibre Toxicol.*, 2012, **9**, 17.
44 T. Zhang, M. Tang, L. Kong, H. Li, T. Zhang, S. Zhang, Y. Xue and Y. Pu, *J. Hazard. Mater.*, 2012, **219–220**, 203–212.
45 Y. Jiang, H. Zhang, Y. Wang, M. Chen, S. Ye, Z. Hou and L. Ren, *PLoS One*, 2013, **8**, e65756.
46 A. Magrez, S. Kasas, V. Salicio, N. Pasquier, J. W. Seo, M. Celio, S. Catsicas, B. Schwaller and L. Forró, *Nano Lett.*, 2006, **6**, 1121–1125.
47 A. K. Patlolla, S. M. Hussain, J. J. Schlager, S. Patlolla and P. B. Tchounwou, *Environ. Toxicol.*, 2010, **25**, 608–621.
48 G. Cirillo, O. Vittorio, S. Hampel, U. G. Spizzirri, N. Picci and F. Iemma, *Int. J. Pharm.*, 2013, **446**, 176–182.
49 L. He, T. He, S. Farrar, L. Ji, T. Liu and X. Ma, *Cell. Physiol. Biochem.*, 2017, **44**, 532–553.
50 P. E. Porporato, N. Filigheddu, J. M. B.-S. Pedro, G. Kroemer and L. Galluzzi, *Cell Res.*, 2018, **28**, 265–280.
51 H. Z. Zardini, A. Amiri, M. Shanbedi, M. Maghrebi and M. Baniadam, *Colloids Surf., B*, 2012, **92**, 196–202.